Broadband energy harvesting based on one-to-one internal resonance*

Wen-An Jiang(姜文安)[1], Xin-Dong Ma(马新东)[1], Xiu-Jing Han(韩修静)[1,†], Li-Qun Chen(陈立群)[2,3], and Qin-Sheng Bi(毕勤胜)[1]

[1] *Faculty of Civil Engineering and Mechanics, Jiangsu University, Zhenjiang* 212013, *China*
[2] *School of Science, Harbin Institute of Technology, Shenzhen* 518055, *China*
[3] *Department of Mechanics, Shanghai University, Shanghai* 200072, *China*

(Received 14 April 2020; revised manuscript received 6 July 2020; accepted manuscript online 15 July 2020)

We design an electromechanical transducer harvesting system with one-to-one internal resonance that can emerge a broader spectrum vibrations. The novel harvester is composed of a Duffing electrical circuit coupled to a mobile rod, and the coupling between both components is realized via the electromagnetic force. Approximate analytical solutions of the electromechanical system are carried out by introducing the multiple scales analysis, also the nonlinear modulation equation for one-to-one internal resonance is obtained. The character of broadband harvesting performance are analyzed, the two peaks and one jump phenomenon bending to the right for variation of control parameters are observed. It is shown that an advanced bandwidth over a corresponding linear model that does not possess a modal energy interchange.

Keywords: energy harvesting, internal resonance, broadband, nonlinear modal interactions

PACS: 05.40.–a, 77.65.–j **DOI:** 10.1088/1674-1056/aba5fd

1. Introduction

The issue of energy harvesting has received an active interest during the past decade. To enrich the bandwidth of energy harvester, researchers have developed many significant methods, such as tuned linear resonance frequency,[1] multimodal,[2] cubic nonlinearity,[3–10] bistable,[11–15] tristable,[16] multistable,[17–19] stochastic resonance,[20,21] and internal resonance.[22,33] However, all the internal resonance energy harvesting systems assume that the second modal is approximately twice or thrice its first mode, but no investigation focused on the one-to-one internal resonance. To enhance the family of energy harvesting, this work develops a one-to-one internal resonance energy harvesting to realize wideband vibration.

Electromechanical systems are involved in many engineering devices, such as vibrating sieves,[34] industrial mixers,[35] industrial shakers,[36] and hydro-turbine systems.[37] Much research has been carried out to understand the dynamical behaviors of such systems which lead to various interesting phenomena such as frequency entrainment,[38] harmonic oscillations,[39] chaotic behavior,[40] feedback control[41] and bursting oscillations.[42] One-to-one internal resonance has been the subject of great deal of recent research. Physical systems with a one-to-one frequency relationship have been extensively reported. Some of these systems, such as the buckled beams,[43] composite laminated rectangular plates[44–51] and nanoresonators.[52] Nevertheless, one-to-one internal resonance harvesting is not found.

In this work, we establish an innovative energy harvesting via the one-to-one internal resonance. An electromechanical transducer energy harvester with such a resonance is designed. Then the equations of the electromechanical coupling system is established. The motion response of the system is computed and the study demonstrates that such an internal resonance owns an advanced frequency bandwidth.

2. Proof of concept

The model of an electromechanical transducer energy harvester, as shown in Fig. 1, consists of a Duffing electrical oscillator magnetically coupled to an attached linear mechanical oscillator via an electromechanical coupling mechanism. By introducing Kirchhoff's voltage law for the circuit part and Newton's second law for the mechanical part, the motion equations of the electromechanical coupling system can be written as

$$L_{\mathrm{ind}1}\ddot{q}+R_1\dot{q}+\frac{q}{C_0}+a_3q^3+lB_1\dot{x}=V_0\cos(\Omega\tau), \quad (1)$$

$$m\ddot{x}+c\dot{x}+kx-lB_1\dot{q}+B_2IL_{\mathrm{coil}}=0, \quad (2)$$

$$L_{\mathrm{ind}2}\dot{I}+R_2I-B_2L_{\mathrm{coil}}\dot{x}=0, \quad (3)$$

where the electrical charge is described by $q(t)$, C_0 is the linear coefficient of the capacitor, a_3 is a non-linear coefficient,

*Project supported by the National Natural Science Foundation of China (Grant Nos. 11632008 and 11702119), the Natural Science Foundation of Jiangsu Province, China (Grant No. BK20170565), China Postdoctoral Science Foundation (Grant No. 2020M671353), and Jiangsu Planned Projects for Postdoctoral Research Funds, China (Grant No. 2020Z376).

†Corresponding author. E-mail: xjhan@mail.ujs.edu.cn

the resistor is represented by $R_{1,2}$, the inductor is defined by $L_{\text{ind1,2}}$, the magnetic intensity is presented via $B_{1,2}$, and l is the length of the interaction between magnetic intensity B_1 and the mobile rods. The mass of mobile beam is m with a spring k, the mechanical motion of the beam is employed by the variable $x(t)$, the mechanical damping is fixed as c, the output current harvested in the coupled system is given by I, and the coil length is denoted by L_{coil}. Finally the amplitude and frequency of the harmoniously external voltage source are depicted by V_0 and Ω, respectively.

Note that the driving force described in Fig. 1 is a harmoniously voltage excitation, and the nonlinear capacitor is realized via the varactor diode.[39] The nonlinear term is proposed by introducing a capacitor represented by Fig. 2, an amplifier is utilized to increase the amplitude of the electric signal. The coupled term $lB_1\dot{x}$ in the circuit equation (1) is the Lorenz electromechanical force, the coupled term $lB_1\dot{q}$ in the mechanical equation (2) is the Laplace force, and the $B_2 I L_{\text{coil}}$ term is the electro-magnetic force which is produced by the coil through the magnetic field. The device is feasible and available in electromechanical engineering.[38–42] Moreover, the model shown in Fig. 1 has also been verified by experiment in Refs. [40,41].

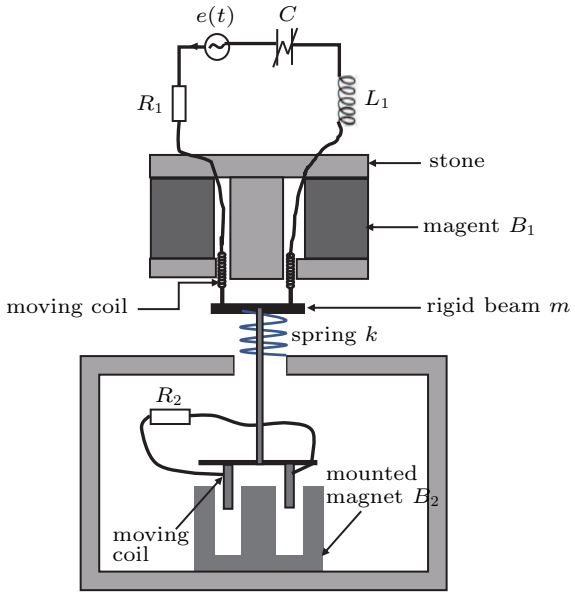

Fig. 1. Schematic diagram of the electromechanical transducer vibratory energy harvesters.

The charge–voltage characteristics represented in Fig. 2 can be written as[42]

$$V_C = \frac{q}{C_1} + nV_{C0}\sinh^{-1}\left(-\frac{q}{2R_C i_0 C_2}\right), \tag{4}$$

where V_{C0} denotes the room temperature, i_0 represents the reverse saturation current, $C_{1,2}$ describe the capacitor.

Consider a small charge in the circuit, the nonlinear item in Eq. (4) can be expanded as[42]

$$V_C = \frac{q}{C_0} + a_3 q^3, \tag{5}$$

where $\frac{1}{C_0} = \frac{1}{C_1} - \frac{nV_{C0}}{2R_C i_0 C_2}$ and $a_3 = \frac{nV_{C0}}{48R_C^3 i_0^3 C_2^3}$.

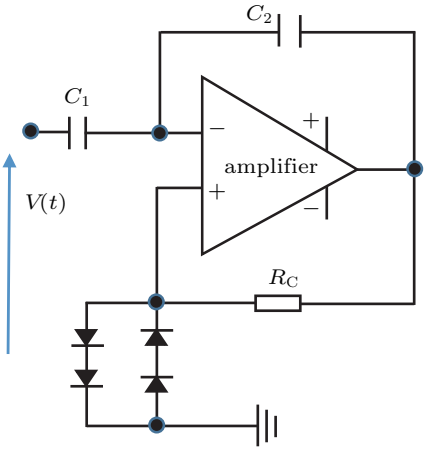

Fig. 2. Model of nonlinear capacitor.[42]

The coupled differential Eqs. (1)–(3) can be simplified to the following dimensionless equations:

$$\ddot{y}_1 + \varsigma_1\dot{y}_1 + y_1 + \alpha y_1^3 + \lambda_1\dot{y}_2 = f\cos(\omega t), \tag{6}$$

$$\ddot{y}_2 + \varsigma_2\dot{y}_2 + \eta y_2 - \lambda_2\dot{y}_1 + \lambda_3 y_3 = 0, \tag{7}$$

$$\dot{y}_3 + \chi y_3 - \dot{y}_2 = 0, \tag{8}$$

where

$$y_1 = \frac{q}{Q_0},\quad y_2 = \frac{x}{l},\quad y_3 = \frac{L_{\text{ind2}}}{B_2 L_{\text{coil}} l} I,$$

$$t = \tau\omega_1,\quad \omega = \frac{\Omega}{\omega_1},\quad \omega_1^2 = \frac{1}{C_0 L_{\text{ind1}}},$$

$$\omega_2^2 = \frac{k_1}{m},\quad \varsigma_1 = \frac{R_1}{\omega_1 L_{\text{ind1}}},\quad \alpha = a_3 C_0 Q_0^2,$$

$$\lambda_1 = \frac{l^2 B_1}{Q_0\omega_1 L_{\text{ind1}}},\quad f = \frac{V_0 C_0}{Q_0},$$

$$\varsigma_2 = \frac{c}{m\omega_1},\quad \eta = \frac{\omega_2}{\omega_1},\quad \lambda_2 = \frac{B_1 Q_0}{m\omega_1},$$

$$\lambda_3 = \frac{B_2^2 L_{\text{coil2}}^2}{m\omega_1^2 L_{\text{ind2}}},\quad \chi = \frac{R_2}{\omega_1 L_{\text{ind2}}}.$$

3. The multiple-scale analysis

We introduce the small transformations of the damping, the external excitation, the non-linearity and the coupling coefficients as follows:

$$\zeta_i \leftrightarrow \varepsilon\zeta_i,\quad f \leftrightarrow \varepsilon f,\quad \alpha \leftrightarrow \varepsilon\alpha,\quad \lambda_i \leftrightarrow \varepsilon\lambda_i. \tag{9}$$

For the case of one-to-one internal resonance accompanied by primary resonance, we put

$$\omega = 1 + \varepsilon\sigma_0,\quad \eta = 1 + \varepsilon\sigma_1, \tag{10}$$

where σ_0 and σ_1 are detuning parameters.

Employing the method of multiple scales to Eqs. (6)–(8), we can approximate the system solution as

$$y_1(t;\varepsilon) = y_{11}(T_0, T_1) + \varepsilon y_{12}(T_0, T_1) + O\left(\varepsilon^2\right),$$

$$y_2(t;\varepsilon) = y_{21}(T_0,T_1) + \varepsilon y_{22}(T_0,T_1) + O(\varepsilon^2),$$
$$y_3(t;\varepsilon) = y_{31}(T_0,T_1) + \varepsilon y_{32}(T_0,T_1) + O(\varepsilon^2). \quad (11)$$

The time derivatives turn into

$$\frac{\mathrm{d}}{\mathrm{d}t} = D_0 + \varepsilon D_1 + \cdots, \quad \frac{\mathrm{d}^2}{\mathrm{d}t^2} = D_0^2 + 2\varepsilon D_0 D_1 + \cdots, \quad (12)$$

where $D_j(j=1,2) = \partial/\partial T_j$.

Setting Eqs. (9)–(12) into Eqs. (6)–(8) and equating terms of ε^0 and ε^1 under the generating equations yield

$$\begin{aligned} &D_0^2 y_{11} + y_{11} = 0,\\ &D_0^2 y_{21} + \eta^2 y_{21} = 0,\\ &D_0 y_{31} + \chi y_{31} = D_0 y_{21}, \end{aligned} \quad (13)$$

$$\begin{aligned} D_0^2 y_{12} + y_{12} &= -2D_0D_1y_{11} - \varsigma_1 D_0 y_{11} - \alpha y_{11}^3\\ &\quad - \lambda_1 D_0 y_{21} + f\cos\omega t,\\ D_0^2 y_{22} + \eta^2 y_{22} &= -2D_0D_1y_{21} - \varsigma_2 D_0 y_{21} + \lambda_2 D_0 y_{11} - \lambda_3 y_{31},\\ D_0 y_{32} + \chi y_{32} &= D_0 y_{22} + D_1 y_{21} - D_1 y_{31}. \end{aligned} \quad (14)$$

The general response of linear Eq. (13) is indicated as

$$\begin{aligned} y_{11} &= A_1(T_1)\exp(\mathrm{i}T_0) + \text{c.c.},\\ y_{21} &= A_2(T_1)\exp(\mathrm{i}\eta T_0) + \text{c.c.},\\ y_{31} &= \frac{\mathrm{i}\eta A_2(T_1)}{\chi + \mathrm{i}\eta}\exp(\mathrm{i}\eta T_0) + B(T_1)\exp(-\chi T_0) + \text{c.c.} \end{aligned} \quad (15)$$

Taking Eqs. (10) and (15) into Eq. (14) and erasing the secular terms, one has

$$\begin{aligned} D_1A_1 &= \Gamma_{11}A_1 + \Gamma_{12}A_1^2\bar{A}_1 + \Gamma_{13}A_2\exp[\mathrm{i}(\eta-1)T_0]\\ &\quad + f\Gamma_{14}\exp[i(\omega-1)T_0],\\ D_1A_2 &= \Gamma_{21}A_2 + \Gamma_{22}A_1\exp[\mathrm{i}(1-\eta)T_0], \end{aligned} \quad (16)$$

where

$$\Gamma_{11} = -\frac{\varsigma_1}{2}, \quad \Gamma_{12} = -\frac{3\alpha}{2i}, \quad \Gamma_{13} = -\frac{\eta\lambda_1}{2}, \quad \Gamma_{14} = \frac{1}{4\mathrm{i}},$$
$$\Gamma_{21} = -\frac{1}{2}\left(\varsigma_2 + \frac{\lambda_3}{\chi+\mathrm{i}\eta}\right), \quad \Gamma_{22} = \frac{\lambda_2}{2\eta}.$$

Employing the functions $A_n(T_1)$ $(n=1,2)$ in the polar form

$$A_n(T_1) = \frac{1}{2}a_n(T_1)\exp[\mathrm{i}\theta_n(T_1)]. \quad (17)$$

Taking Eq. (17) into Eq. (16), one explicitly has

$$\begin{aligned} D_1a_1 &= \mathrm{Re}(\Gamma_{11})a_1 + \frac{1}{4}a_1^3\mathrm{Re}(\Gamma_{12})\\ &\quad + a_2[\mathrm{Re}(\Gamma_{13})\cos\gamma_1 - \mathrm{Im}(\Gamma_{13})\sin\gamma_1]\\ &\quad + 2f[\mathrm{Re}(\Gamma_{14})\cos\gamma_2 - \mathrm{Im}(\Gamma_{14})\sin\gamma_2], \end{aligned} \quad (18)$$

$$D_1a_2 = \mathrm{Re}(\Gamma_{21})a_2 + a_1[\mathrm{Re}(\Gamma_{22})\cos\gamma_1 + \mathrm{Im}(\Gamma_{22})\sin\gamma_1], \quad (19)$$

$$\begin{aligned} D_1\gamma_1 &= \sigma_1 + \mathrm{Im}(\Gamma_{21}) - \frac{a_1}{a_2}[\mathrm{Re}(\Gamma_{22})\sin\gamma_1\\ &\quad - \mathrm{Im}(\Gamma_{22})\cos\gamma_1] - \mathrm{Im}(\Gamma_{11})\\ &\quad - \frac{1}{4}a_1^2\mathrm{Im}(\Gamma_{12}) - \frac{a_2}{a_1}[\mathrm{Re}(\Gamma_{13})\sin\gamma_1 + \mathrm{Im}(\Gamma_{13})\cos\gamma_1]\\ &\quad - \frac{2f}{a_1}[\mathrm{Re}(\Gamma_{14})\sin\gamma_2 + \mathrm{Im}(\Gamma_{14})\cos\gamma_2], \end{aligned} \quad (20)$$

$$\begin{aligned} D_1\gamma_2 &= \sigma_0 - \mathrm{Im}(\Gamma_{11}) - \frac{1}{4}a_1^2\mathrm{Im}(\Gamma_{12})\\ &\quad - \frac{a_2}{a_1}[\mathrm{Re}(\Gamma_{13})\sin\gamma_1 + \mathrm{Im}(\Gamma_{13})\cos\gamma_1]\\ &\quad - \frac{2f}{a_1}[\mathrm{Re}(\Gamma_{14})\sin\gamma_2 + \mathrm{Im}(\Gamma_{14})\cos\gamma_2], \end{aligned} \quad (21)$$

where

$$\gamma_1 = \theta_2 - \theta_1 + \sigma_1 T_1, \quad \gamma_2 = \sigma_0 T_1 - \theta_1.$$

To proceed further we discuss the steady-state response, and find

$$\begin{aligned} 0 &= \mathrm{Re}(\Gamma_{11})a_1 + \frac{1}{4}a_1^3\mathrm{Re}(\Gamma_{12})\\ &\quad + a_2[\mathrm{Re}(\Gamma_{13})\cos\gamma_1 - \mathrm{Im}(\Gamma_{13})\sin\gamma_1]\\ &\quad + 2f[\mathrm{Re}(\Gamma_{14})\cos\gamma_2 - \mathrm{Im}(\Gamma_{14})\sin\gamma_2], \end{aligned} \quad (22)$$

$$0 = \mathrm{Re}(\Gamma_{21})a_2 + a_1[\mathrm{Re}(\Gamma_{22})\cos\gamma_1 + \mathrm{Im}(\Gamma_{22})\sin\gamma_1], \quad (23)$$

$$\begin{aligned} 0 &= \sigma_1 + \mathrm{Im}(\Gamma_{21}) - \frac{a_1}{a_2}[\mathrm{Re}(\Gamma_{22})\sin\gamma_1\\ &\quad - \mathrm{Im}(\Gamma_{22})\cos\gamma_1] - \mathrm{Im}(\Gamma_{11})\\ &\quad - \frac{1}{4}a_1^2\mathrm{Im}(\Gamma_{12}) - \frac{a_2}{a_1}[\mathrm{Re}(\Gamma_{13})\sin\gamma_1 + \mathrm{Im}(\Gamma_{13})\cos\gamma_1]\\ &\quad - \frac{2f}{a_1}[\mathrm{Re}(\Gamma_{14})\sin\gamma_2 + \mathrm{Im}(\Gamma_{14})\cos\gamma_2], \end{aligned} \quad (24)$$

$$\begin{aligned} 0 &= \sigma_0 - \mathrm{Im}(\Gamma_{11}) - \frac{1}{4}a_1^2\mathrm{Im}(\Gamma_{12})\\ &\quad - \frac{a_2}{a_1}[\mathrm{Re}(\Gamma_{13})\sin\gamma_1 + \mathrm{Im}(\Gamma_{13})\cos\gamma_1]\\ &\quad - \frac{2f}{a_1}[\mathrm{Re}(\Gamma_{14})\sin\gamma_2 + \mathrm{Im}(\Gamma_{14})\cos\gamma_2]. \end{aligned} \quad (25)$$

Equations (22)–(25) determine the modulation relationships between response and frequency. To calculate these solutions, we numerically compute the generating nonlinear algebraic equations by the Mathematica software. In the meantime, the output current response can be established as

$$y_3 = \frac{\eta}{\sqrt{\chi^2+\eta^2}}a_2. \quad (26)$$

To consider the stability of the responses, we write the disturbance equation as

$$\begin{aligned} &\left(D_1\Delta a_1 \;\; D_1\Delta a_2 \;\; D_1\Delta\gamma_1 \;\; D_1\Delta\gamma_2\right)^{\mathrm{T}}\\ &= \boldsymbol{J}\left(\Delta a_1 \;\; \Delta a_2 \;\; \Delta\gamma_1 \;\; \Delta\gamma_2\right)^{\mathrm{T}}, \end{aligned} \quad (27)$$

where superscript T defines transpose and $\boldsymbol{J}$ describes the Jacobian matrix. The motion response is stable when all the eigenvalues possess negative real parts, or the corresponding motion is unstable.

4. Influence of the design parameters

Since the most important attribution of energy harvesting is the collected bandwidth, which can enhance the power transduction efficiency of energy harvesters under broadband external ambient environmental excitations, thereby collecting power on a wide spectrum of external frequency is our most pressing problem. In light of this challenge, the amplitude-frequency curves of one-to-one internal resonance will be discussed in this section. To describe the influence of the design parameters, we plot three sets of response curves in Figs. 3–8 for six physical parameters. The geometric characteristics of the energy harvester are denoted as $m = 0.05$ kg, $C_0 = 2200$ μF, $Q_0 = 0.1C$, $a_3 = 43182$ V/C^3, $c = 0.1016$ N·m/s, $L_{\text{ind1}} = 1.1$ H, $B_1 = 20$ T, $l = 0.2$ m, $R_1 = 1.118$ Ω, $R_2 = 20.3279$ Ω, $B_2 = 1$ T, $L_{\text{ind2}} = 1$ H, $L_{\text{coil}} = 2$ m and $V_0 = 10$ V. Consequently, one-to-one internal resonance occurs together with $\omega_1 = 20.3279$ s^{-1} and $\omega_2 = 20.3279$ s^{-1}. Moreover, the internal detuning value σ_1 is zero. The motion response curves will be plotted in the following figures, where solid lines denote stable vibrations and dotted lines employ the unstable motions.

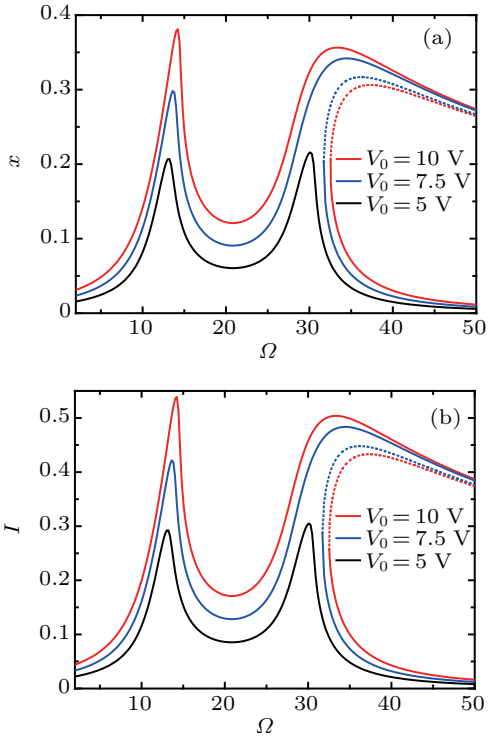

Fig. 3. Frequency-resonance curves for different amplitudes of voltage source.

Having observed the favorable effect of excitation levels on the response of system, Fig. 3 shows the frequency response curves of one-to-one internal resonance for three different amplitudes of external voltage source ($V_0 = 10$ V, 7.5 V and 5 V), in which the height and the bandwidth are increased when the amplitudes of external voltage source is extended. There are obviously two mountain peaks in the response curves, also the motion curves have a multi-valued regions. Subsequently, there is one peak bending to the right indicating a hardening-type nonlinearity. This is because the modal interactions under the one-to-one internal resonance can result in an energy exchange between the first modal frequency and the second mode. In the meantime, the two mountain peaks and the jumping bring about broadband energy harvesting. In addition, the motion amplitude and the response bandwidth increase with the voltage source. In energy harvesting, the broadband feature of resonance frequency is desired.

Figure 4 depicts the frequency response curve of one-to-one internal resonance with three different levels of cubic nonlinear coefficients ($a_3 = 43182$ V/C^3, 32387 V/C^3 and 21591 V/C^3). In Fig. 4, as nonlinearity is decreased, the response amplitude of left peak is increased slightly, while the response amplitude of right peak is increased obviously. In addition, the bandwidth is extended obviously. Consequently, in the one-to-one internal resonance energy harvesting, decrease in the cubic nonlinear terms becomes more significant. It is worth noticing that the result is different from the classical single degree of freedom Duffing energy harvester.[3–10]

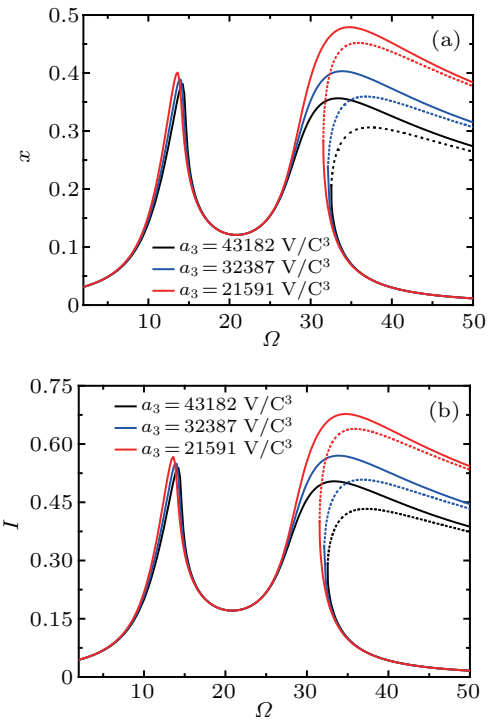

Fig. 4. Frequency-resonance curves for different cubic nonlinear coefficients.

Figure 5 plots the frequency response curve of one-to-one internal resonance with three different resistors ($R_1 = 1.118$ Ω, 2.236 Ω and 3.354 Ω). The frequency response diagrams of displacement and current show that the influence of one-to-one internal resonance becomes more pronounced with reduced resistors. In addition to the increase in the mountain peak motion amplitude, the bandwidth of stable solutions also increases as

the resistors is decreased. Therefore, light resistors are preferred for enhanced bandwidth of effective operation for the harvester with one-to-one internal resonance.

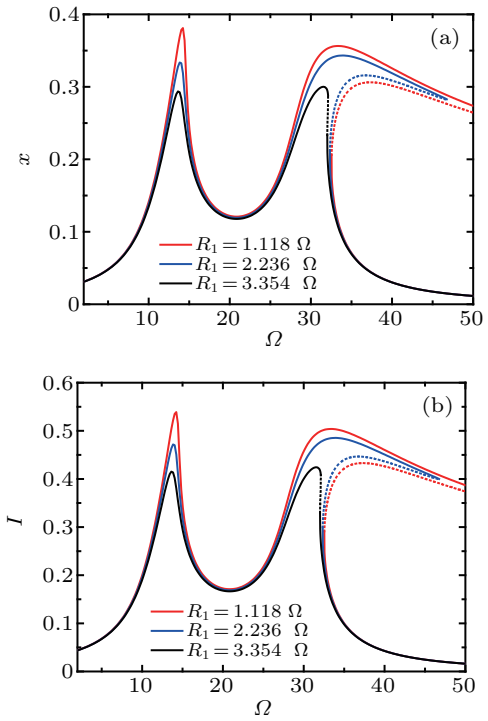

Fig. 5. Frequency-resonance curves for different resistors R_1.

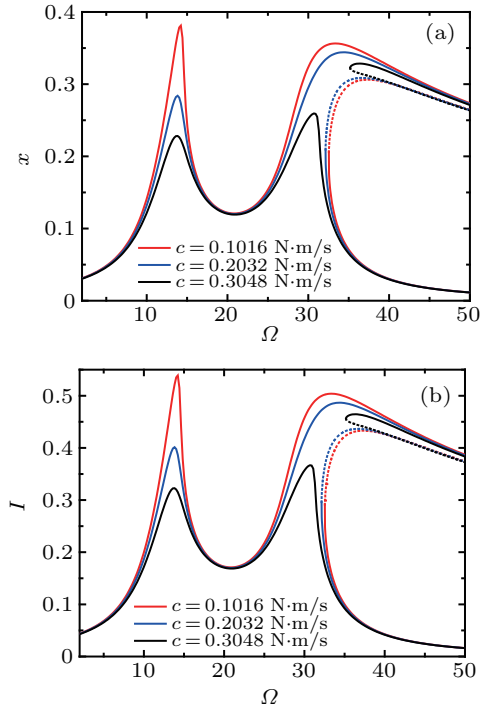

Fig. 6. Frequency-resonance curves for different damping coefficients.

Figure 6 shows the frequency response curve of one-to-one internal resonance along with different damping values ($c = 0.1016$ N·m/s, 0.2032 N·m/s and 0.3048N·m/s). In Fig. 6, as the damping coefficient c increases, the peak height and the bandwidth are decreased.

Figure 7 plots the frequency response curve of one-to-one internal resonance with different magnetic strengths B_1 ($B_1 = 5$ T, 10 T and 20 T). The results indicate that the peak and the bandwidth of displacement and current frequency response curves increase monotonically with increasing magnetic strengths B_1.

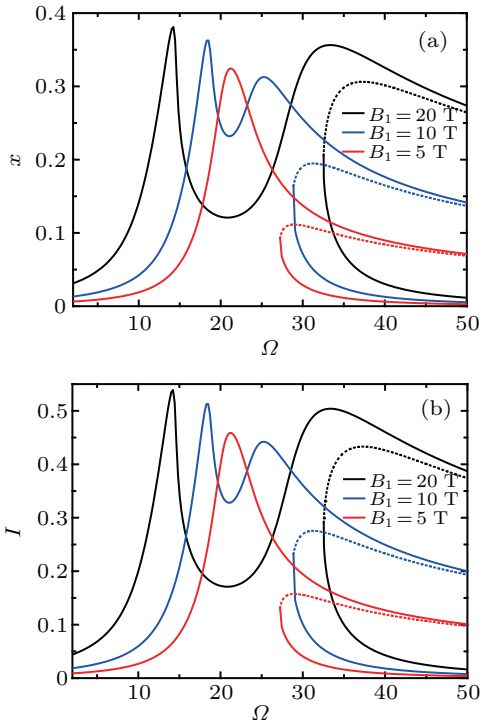

Fig. 7. Frequency-resonance curves for different magnetic strengths B_1.

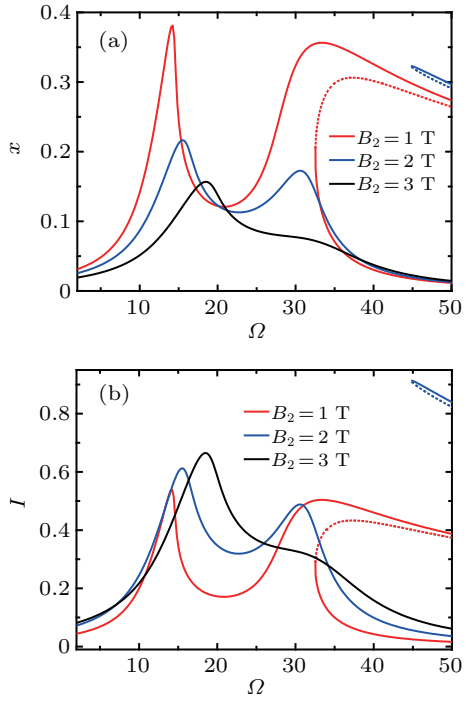

Fig. 8. Frequency-resonance curves for different magnetic strengths B_2.

Figure 8 depicts the frequency response curve of one-to-one internal resonance with different magnetic strengths B_2

($B_2 = 1$ T, 2 T and 3 T). The results indicate that the peak height and the bandwidth of displacement frequency response curves increase with decreasing magnetic strengths B_2. In addition, as the magnetic strengths B_2 is decreased, the bandwidth of current frequency response curves is increased, while the peak of current frequency response is decreased slightly.

5. Performance comparison of the internal resonance and the linear configurations

Having observed the broadband electromechanical response of the one-to-one internal resonance electromechanical transducer coupling a linear oscillator energy harvester described by Eqs. (1)–(3), comparisons can be made against the conventional linear configuration.

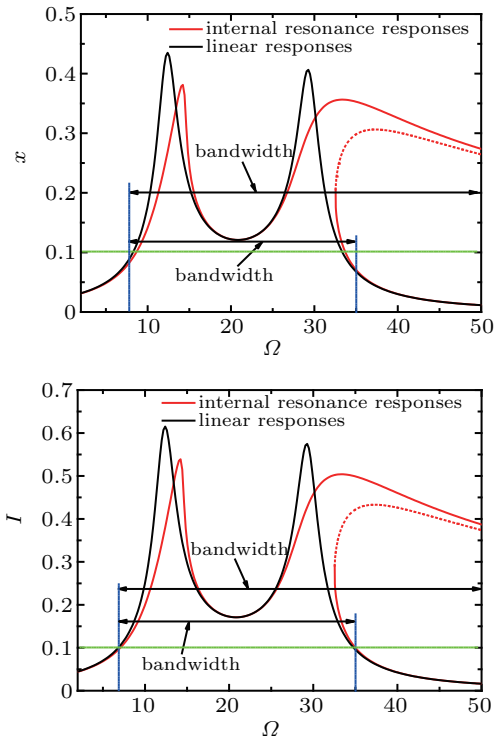

Fig. 9. Comparison of the internal resonance and the linear results.

The electromechanical equations of the linear RLC circuit with a linear oscillator energy harvester are

$$L_{\text{ind1}}\ddot{q} + R_1\dot{q} + \frac{q}{C_0} + lB_1\dot{x} = V_0\cos(\Omega\tau), \tag{28}$$

$$m\ddot{x} + c\dot{x} + kx - lB_1\dot{q} + B_2 I L_{\text{coil}} = 0, \tag{29}$$

$$L_{\text{ind2}}\dot{I} + R_2 I - B_2 L_{\text{coil}}\dot{x} = 0. \tag{30}$$

For the same system parameters, initial conditions, and the forcing amplitude of the one-to-one internal resonance harvester, one can calculate the frequency motion diagrams of the linear configuration via Eqs. (28)–(30). Figure 9 shows the motion response diagrams of one-to-one internal resonance and the linear configurations. In the meantime, we suppose that a minimum steady-state current of 0.1 A should be kept during the system operation, and the corresponding bandwidth of frequency response is defined under the minimum current. As can be seen from the steady-state motion responses appearing in this figure, the bandwidth of the one-to-one internal resonance harvester can be much larger than that of the linear configuration.

6. Numerical validation

To confirm the accuracy of approximately analytical steady-state values, Eqs. (6)–(8) are numerically calculated by utilizing the fourth-order Runge–Kutta algorithm. Numerical values from Eqs. (6)–(8) are recorded in Fig. 10 as red solid dots. Investigating Fig. 10, the steady-state responses from the analysis and the simulation have the greater consistency. In the meantime, the simulation values show the jumping phenomena emerged in the primary resonance and one-to-one internal resonances of electromechanical transducer electromagnetic harvester.

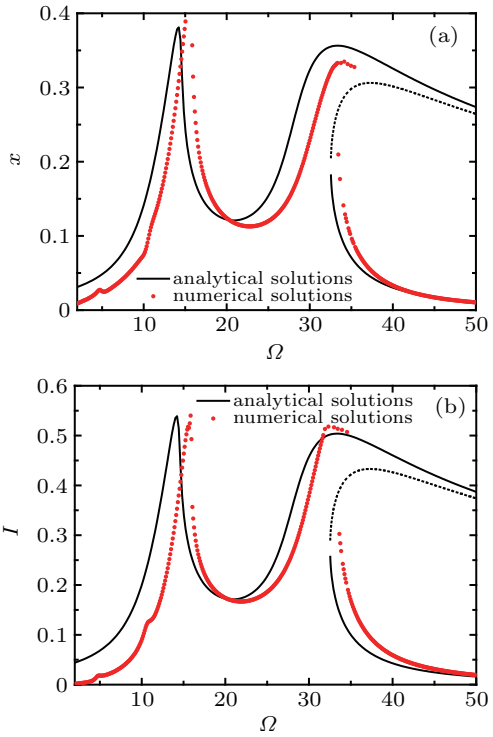

Fig. 10. Comparison of the analytical and the numerical results.

7. Conclusions

We have confirmed that developing multimodal nonlinear energy harvester coupling with one-to-one internal resonance can be employed to extend the steady-state bandwidth of the harvester. As a simple proof, an electromechanical transducer energy harvester along with a linear oscillator is exploited to address one-to-one internal resonance. Specifically, the multiple-scale analysis is utilized to employ the motion response, and compared the performance of the presented internal resonance model and the correspond linear location. The

accuracy of approximately analytical values is checked via numerical integration. The investigation acquires the following observations.

(1) An electromechanical transducer shaped energy harvester constructed by a nonlinear RLC circuit is utilized to realize one-to-one internal resonance.

(2) The motion responses are analytically observed to predict two peaks and one jump phenomenon, one peak bending to the right implicating a hardening nonlinearity.

(3) The amplitude and the bandwidth of motion response increase with the excitation amplitudes of voltage source and magnetic strengths B_1, while decrease with increasing cubic nonlinear coefficients a_3, resistor R_1, damping coefficient c, and magnetic strengths B_2.

(4) The analytical forecast is supported by the numerical results.

(5) The advancement of the presented internal resonance technique is contrasted with its linear counterparts.

References

[1] Challa V, Prasad M, Shi Y and Fisher F 2008 *Smart Mater. Struct.* **75** 015035
[2] Shahruz S M 2006 *J. Sound Vib.* **292** 987
[3] Fan K Q, Xu C H, Wang W D and Fang Y 2014 *Chin. Phys. B* **23** 084501
[4] Li H T and Qin W Y 2016 *Chin. Phys. B* **25** 110503
[5] Zhang Y W, Wang C, Yuan B and Fang B 2017 *Shock Vib.* **1987456** 1
[6] Yan Z M and Hajj M 2017 *J. Intel. Mat. Syst. Str.* **28** 254
[7] Cao D X, Gao Y H and Hu W H 2019 *Acta Mech. Sinica* **35** 894
[8] Tan T, Yan Z M, Zou Y J and Zhang W M 2019 *Mech. Syst. Signal Pr.* **123** 513
[9] Jiang W A, Sun P, Zhao G L and Chen L Q 2019 *Appl. Math. Mech. -Engl. Ed.* **40** 579
[10] Guo X Y, Wang S B, Sun L and Cao D X 2020 *Acta Mech. Sinica* **36** 234
[11] Cottone F, Vocca H and Gammaitoni L 2009 *Phys. Rev. Lett.* **102** 080601
[12] Wang G Y and Tang L H 2017 *Mech. Syst. Signal Pr.* **86** 29
[13] Zou H X, Zhang W M, Wei K X, Li W B, Peng Z K and Meng G 2016 *J. Appl. Mech.* **83** 121005
[14] Lan C B and Qin W Y 2017 *Mech. Syst. Signal Pr.* **85** 71
[15] Zhou Z Y, Qin W Y, Du W F, Zhu P and Liu Q 2019 *Mech. Syst. Signal Pr.* **115** 162
[16] Cao J Y, Zhou S X, Wang W and Lin J 2015 *Appl. Phys. Lett.* **106** 173903
[17] Zhou Z Y, Qin W Y and Zhu P 2017 *Mech. Syst. Signal Pr.* **84** 158
[18] Wang B, Zhang Q C, Wang W and Feng J J 2018 *Mech. Syst. Signal Pr.* **112** 305
[19] Yang S and Cao Q J 2019 *J. Stat. Mech.-Theory E* 033405
[20] Li H T and Qin W Y 2015 *Nonlinear Dyn.* **81** 1751
[21] Li H T, Qin W Y, Lan C B, Deng W Z and Zhou Z Y 2016 *Smart Mater. Struct.* **25** 015001
[22] Chen L Q and Jiang W A 2015 *J. Appl. Mech.* **82** 031004
[23] Cao D X, Leadenham S and Erturk A 2015 *Eur. Phys. J. Special Topics* **224** 2867
[24] Jiang W A, Chen L Q and Ding H 2016 *Nonlinear Dyn.* **85** 2507
[25] Chen L Q, Jiang W A, Panyam M and Daqaq M F 2016 *J. Acoust Vib.* **138** 061007
[26] Wu Y P, Ji H L, Qiu J H and Han L 2017 *Sens. Actuators A-Phys.* **264** 1
[27] Yang W and Towfighian S 2017 *Smart Mater. Struct.* **26** 095008
[28] Yang W and Towfighian S 2017 *Mech. Syst. Signal Pr.* **90** 317
[29] Rocha R T, Balthazar J M, Tusset A M, Piccirillo V and Felix J L P 2017 *Meccanica* **52** 2583
[30] Xiong L Y, Tang L T and Mace B R 2018 *Nonlinear Dyn.* **91** 1817
[31] Liu H J and Gao X M 2019 *Nonlinear Dyn.* **96** 1067
[32] Nie X C, Tan T, Yan Z M, Yan Z T and Hajj M R 2019 *Int. J. Mech. Sci.* **159** 287
[33] Pan J N, Qin W Y, Deng W Z and Zhou H L 2019 *Chin. Phys. B* **28** 017701
[34] Tcheutchoua F D and Woafo P 2011 *J. Vib. Acoust.* **133** 061018
[35] Jerrelind J and Stensson A 2000 *Chaos Solit. Fract.* **11** 2413
[36] Wang Z and Chau K T 2008 *Chaos Solit. Fract.* **36** 694
[37] Zhang H, Chen D, Xu B and Wang F 2015 *Energy Convers. Manage.* **90** 128
[38] Yamapi R, Orou J B and Woafo P 2003 *J. Sound Vib.* **259** 1253
[39] Mogo J B and Woafo P 2007 *J. Comput. Nonlinear Dyn.* **2** 374
[40] Kitio KC A, Nana B and Woafo P 2010 *J. Sound Vib.* **329** 3137
[41] Domguia U S, Abobda L T and Woafo P 2016 *J. Comput. Nonlin. Dyn.* **11** 051006
[42] Simo H and Woafo P 2011 *Mech. Res. Commun.* **38** 537
[43] Emam S A and Nayfeh A H 2013 *Int. J. Nonlin. Mech.* **52** 12
[44] Zhang W, Yang J H, Zhang Y F and Yang S W 2019 *Eng. Struct.* **198** 109501
[45] Zhang W, Liu Y Z and Wu M Q 2019 *Compos. Struct.* **225** 111140
[46] Zhang Y F, Zhang W and Yao Z G 2018 *Eng. Struct.* **173** 89
[47] Yao M H, Ma L and Zhang W 2018 *Sci. Chin. E* **61** 1404
[48] Yao M H, Zhang W and Yao Z G 2015 *J. Vib. Acoust.* **137** 011002
[49] Zhang W, Zhang J H, Yao M H and Yao Z G 2010 *Acta Mech.* **211** 23
[50] Zhang W, Yao Z G and Yao M H 2009 *Sci. China Ser. E* **52** 731
[51] Zhang W and Zhao M H 2012 *Nonlinear Dyn.* **70** 295
[52] Nathamgari S P, Dong S Y and Medina L 2019 *Nano Lett.* **19** 4052